



Possibility of Spin-polarized Transport in Edge Fluorinated Armchair Boron Nitride Nanoribbons

Journal:	<i>RSC Advances</i>
Manuscript ID	RA-ART-10-2015-021832.R1
Article Type:	Paper
Date Submitted by the Author:	28-Dec-2015
Complete List of Authors:	Rai, Hari; IIT Indore, Saxena, Shailendra; IIT Indore, Physics Mishra, Vikash; IIT Indore, Physics Late, Ravikiran; IIT Indore, ; Kumar, Rajesh; Indian Institute of Technology Indore, Physics Sagdeo, Pankaj; IIT Indore, Physics Jaiswal, Neeraj; PDPM- Indian Institute of Information Technology, Design and Manufacturing, Jabalpur, Physics Srivastava, Pankaj; ABV-IIITM Gwalior, Physics
Subject area & keyword:	Nanoscience - Physical < Physical

Possibility of Spin-polarized Transport in Edge Fluorinated Armchair Boron Nitride Nanoribbons

Hari Mohan Rai¹, Shailendra K. Saxena¹, Vikash Mishra¹, Ravikiran Late¹, Rajesh Kumar¹, Pankaj R. Sagdeo¹,

¹Material Research Laboratory, Discipline of Physics, Indian Institute of Technology Indore, Indore (M.P.) – 452017, India

*Neeraj K. Jaiswal^{*2}*

²Discipline of Physics, PDPM- Indian Institute of Information Technology, Design and Manufacturing, Jabalpur – 482005, India

Pankaj Srivastava³

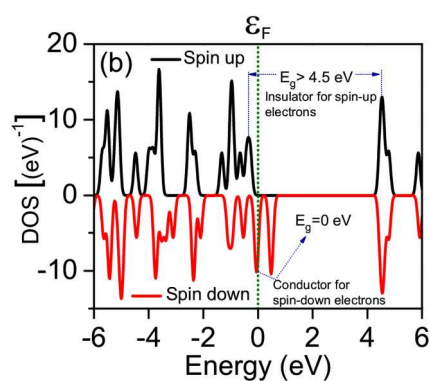
³Computational Nanoscience and Technology Lab. (CNTL), ABV- Indian Institute of Information Technology and Management, Gwalior – 474015, India

* Corresponding author: pankajs@iiitm.ac.in

ABSTRACT

We predict the possibility of spin based electronic transport in edge fluorinated armchair boron nitride nanoribbons (ABNNRs). The structural stability, electronic and magnetic properties of these edge fluorinated ABNNRs have been systematically analyzed by means of first-principles calculations within the local spin-density approximation (LSDA). Regardless of their width, ABNNRs with F-passivation at only edge-B atoms are found to be thermodynamically stable and half-metallic in nature. The spin polarized states are found to be ~ 0.4 eV more stable than that of spin compensated states. Further, upto 100% spin polarization is expected in ABNNRs with F-passivation at only edge-B atoms as indicated by giant splitting of spin states which is observed in corresponding band structures, DOS and transmission spectrum. The existence of half-metallicity is attributed to the localization of electronic charge at unpassivated edge-N atoms as revealed from the analysis of Bloch states and projected density of states (PDOS). Importantly, present stability analysis suggests that the possibility of experimental realization of spin polarized transport in ABNNRs is more promising via F-passivation of ribbon edges than that of H-passivation. The observed half-metallic nature and large difference in the energies (~ 0.4 eV) of spin polarized and spin compensated states projects these half-metallic ABNNRs as potential candidate for inorganic spintronic applications.

Key words: Boron nitride; nanoribbons; Electronic structure; Density of States.



Calculated DOS for edge-fluorinated ABNNRs; featuring Half-metallicity.

TOC

1. INTRODUCTION

The discovery of single atom thick sheet of hexagonal boron nitride (h-BN) has invigorated theoretical as well as experimental research activities associated with h-BN nanomaterials¹⁻⁴. This quasi-two-dimensional (2D) h-BN sheet has large energy band gap (~5eV) which ensures its stability at elevated temperatures and thus makes it a promising candidate for high temperature semiconductor devices. Some interesting features like capability of dielectric screening,⁵ strong oxidation resistance⁶ and tunable (achieved via creating triangular defects)⁷ magnetic and electronic properties are recently reported in atomically thin BN nanosheets. Quasi-1-D thin strips carved out of h-BN sheet also exhibit excellent structural stability and distinct electronic properties as compared to parent h-BN sheet due to the quantum confinement effects⁴. These strips are formally known as boron nitride nanoribbons (BNNRs). Chen. et al.⁸ have already synthesized hollow BNNRs through evaporation using B–N–O–Fe as precursor and ZnS nanoribbons as templates. Moreover, BNNRs have also been produced experimentally via in-situ unzipping of boron nitride nanotubes (BNNTs)⁹. Similar to their organic counterpart i.e. Graphene Nanoribbons (GNRs), BNNRs can also be fabricated from a single h-BN layer via lithographic patterning¹⁰. According to the definite shape of edges BNNRs are mainly of two type i.e. zigzag boron nitride nanoribbons (ZBNNRs) and armchair boron nitride nanoribbons (ABNNRs). BNNRs exhibit fascinating and outstanding electronic properties similar to that of GNRs, which are crucial for the application in advance devices^{11,12}. For example; Cl adsorption¹³ and PH₃-passivation of ribbon edges¹⁴ significantly modifies electronic state/band gap of ABNNRs which can be useful in gas sensor technology for sensing Cl and PH₃ gas molecules. The electronic band gap (E_g) of ABNNRs passivated by H, oscillates periodically as a function of their width¹⁵ whereas the band gap of ZBNNRs decreases monotonically, with increasing ribbon, width when both the edges are H-passivated^{16,17}. Owing to high efficiency and low power consumption, spintronic devices are attracting considerable attention nowadays. Being the key property for spin transport based electronics, Half-metallicity, has been vastly predicted and studied in different nanostructures¹⁸⁻²⁰ along with many other compounds like alloys (including ternary and quaternary Heusler alloys)²¹⁻²³, double layer perovskites^{24,25}, transition metal pnictides, and chalcogenides in zinc blende phase²⁶⁻²⁸. Recently, the existence of a large spin polarization of $(93^{+8}_{-11})\%$ has been directly evidenced at room temperature in an epitaxial thin film of Co₂MnSi²⁹. First principle calculations have already shown that half-metallicity may be

realized also in BNNRs either by chemically functionalizing zigzag edges with different groups such as H and F or with the application of an external in-plane electric field^{30–32}. In previous study on ZBNNRs¹⁶, it is predicted that one-edge (only B-edge) H-passivation makes the ribbons ‘semi-metallic’ unlike the ‘half-metallic’ as predicted by Zheng et al.³⁰ but in the perspective of spin polarized transport, both of these results might be consistent with each other. Moreover, half-metallicity has also been perceived theoretically in ZBNNRs via percentage hydrogenation³³, hybridization (through carbon in BC₂N nanoribbons)³⁴, and also through structural modifications (e.g., by making stirrup, boat, twist-boat etc.)³⁵. Conversely, in case of ABNNRs, half-metallicity has been predicted in hybrid armchair BCN- nanoribbons³⁶ and also in H-passivated (edge-hydrogenated) ABNNRs³⁷ but the experimental realization of these edge hydrogenated ABNNRs is energetically not favorable as they are thermodynamically less stable³⁷. However, from the perspective of energetically stable spin-polarization, ABNNRs are almost unexplored in comparison with zigzag counterparts. By keeping in view, that ABNNRs can also be potential spintronics elements, this article presents an attempt - to predict the possibility of spin polarized transport in ABNNRs via edge fluorination and to analyze it in detail using DFT calculations.

Here, we predict the possibility of spin polarized transport in ABNNRs when only edge-B atoms are passivated with F atoms. In addition, this article presents a systematic analysis of structural stability, electronic and magnetic properties for fully and partially edge fluorinated ABNNRs with different widths. Present analysis reveals that edge fluorination transforms bare ABNNRs into ferromagnetic/antiferromagnetic half-metals as energetically most favorable structures unlike edge-hydrogenated counterparts^{37,38}.

2. COMPUTATIONAL DETAILS

The first-principles calculations were performed with Atomistix Tool Kit-Virtual NanoLab (ATK-VNL)^{39,40} under the framework of density functional theory (DFT). The exchange correlation energy was approximated by local spin density approximation (LSDA) as proposed by Perdew and Zunger⁴¹. The reason for selecting LDA for present DFT calculations is that the generalized gradient approximation underestimates the surface–impurity interactions⁴². ATK employs an effective potential $V^{eff}[n] = V^H[n] + V^{xc}[n] + V^{ext}$ for calculations. Here, first

two terms exhibit the potential due to interactions with the other electrons (represented in terms of electron density); the first term, $V^H[n]$, is the classical electrostatic potential (also known as Hartree potential) due to the mean-field electrostatic interaction, and the second term, $V^{xc}[n]$, is the exchange-correlation potential caused by the quantum mechanical nature of the electrons. The third term V^{ext} represents external potential which is the sum of ions potentials (represented by norm-conserving pseudo-potentials) and electrostatic interaction of system with an external electrostatic field. For present calculations ABNNRs were modeled with periodic boundary conditions along z -axis, whereas the other two dimensions were confined. Norm-conserving pseudo-potentials with an energy cut off of 100 Ry, was selected for the expansion of plane waves. We implemented double ζ plus polarized basis set for all the calculations. The k -point sampling was selected to be $1 \times 1 \times 100$. In order to avoid artificial inter-ribbon interactions, ribbons were separated using a cell padding vacuum region of 10 Å. All the atoms, in the considered geometries, are relaxed and optimization of atomic positions and lattice parameters has been continued until the forces on each constituent atom reduced upto 0.05 eV/Å. We represent the ribbon-width by a width parameter N_a , defined as the number of B or N atoms³⁷ along the ribbon width as depicted in figure 1, therefore, ABNNR with n B or N atoms across the ribbon is named as n -ABNNR.

3. RESULTS AND DISCUSSION

For present calculations we have considered ABNNRs with – (i) fully F-passivated edges (ABNNR_{FBN}) and (ii) partial/half F-passivated edges. Furthermore, the ABNNRs belonging to latter category are divided into two subgroups i.e., ABNNR_{FB} and ABNNR_{FN} depending upon whether only B or only N edge atoms are passivated by F-atoms respectively. The electronic and magnetic properties of bare ABNNRs have also been investigated and these ribbons were found to be nonmagnetic semiconductors as also predicted by Ding *et al.*³⁸. In order to take size effects into considerations, we investigate ABNNRs having widths $N_a = 6$ to 10. Since the findings are qualitatively similar for symmetric ribbons (Odd- N_a), we displayed the figures only for ABNNRs with $N_a = 9$. Figure 1 schematically represents optimized geometry of ABNNR in all considered ribbon configurations with $N_a = 9$ as representative case. The convention of super cell, used for simulation, is also depicted in the same figure for various ribbon structures.

3.1 Stability analysis

First of all, in order to examine the relative stability of considered ribbon configurations, cohesive energy (E_c) has been calculated by using the following relation;

$$E_c = \frac{1}{(p+q+r)} \left[E_{tot}^{ABNNR} - (pE_{atom}^B + qE_{atom}^N + rE_{atom}^F) \right] \quad (1)$$

where E_{tot}^{ABNNR} , E_{atom}^B , E_{atom}^N and E_{atom}^F are the total energies of ABNNR, free B atom, N atom and F atom, respectively; p, q and r are the number of B, N and F atoms respectively in the super cell. The cohesive energies calculated for considered ribbon structures are summarized in Table I. It is noticeable that lower values of E_c favor higher stability. The perusal of Table I indicates that irrespective of their width ABNNR_{FB} are energetically most stable ribbon structures amongst all considered configurations and the minimum difference in E_c is found to be 330 meV which is observed for 10-ABNNR_{FB} and 10-ABNNR_{FN} structures. This difference is large enough for a room temperature operation. Further, the energy difference is more pronounced at narrow widths whereas wider ribbons are found to be relatively more stable [Table 1]. This indicates that amount of stress in the nanoribbons, which causes structural instability, is inversely proportional to the ribbon width. Present stability analysis predicts that amongst all investigated edge fluorinated ABNNRs; the possibility of experimental realization is highest for ABNNR_{FB} structures as they have lowest E_c . It is noticeable that we observed a mild reconstruction at the outer edges of ribbons when only B/N edge-atoms are saturated with F (i.e., ABNNR_{FB} and ABNNR_{FN}). Owing to this edge reconstruction the bond length of the outer edge B-N bond is slightly reduced (1.37 Å) as compared to the normal bond length (1.38Å) which provides stability to these ribbon structures in a similar way to that of edge reconstructed GNRs where edge reconstruction was responsible for the edge stability of bare GNRs⁴³. In addition, it should be noted as an extra information that edge-fluorinated ZBNNRs are energetically more favorable than that of edge-fluorinated ABNNRs as corresponding cohesive and binding energies are tabulated in supplementary information (Table S1 and Table S2). Moreover, it has been already reported that H-passivation (hydrogenation) of only B edge atoms (ABNNR_{HB}) makes armchair ribbons half-metallic³⁷ but higher value of E_c restricts their experimental realization because in case of edge hydrogenation, armchair ribbons with H-passivation at only N edge atoms (ABNNR_{HN}) were found relatively more stable (as the value of corresponding E_c was found to be

lowest) than that of $ABNNR_{HB}$ ³⁷. Importantly, in the present case of edge-fluorination (F-passivation); armchair ribbons with F-passivation at only B edge-atoms are found to be half-metallic and most stable ($ABNNR_{FB}$) amongst all presently investigated ribbon configurations. In addition to this E_c analysis, binding energy (E_b) per passivator-atom has also been calculated to further verify the stability (i.e., the probability of experimental realization of passivation) of bonding between Passivator atoms and host edge B/N atoms. For this purpose, both, F and H-atoms are used separately as edge-passivators in different ribbon configurations and E_b per F (or H)-atom is calculated by using following formula-

$$E_B = \frac{1}{x} \left[E_{tot}^{Configuration} - E_{tot}^{Bare} - xE_{tot}^{F(orH)} \right]$$

Where $E_{tot}^{Configuration}$, E_{tot}^{Bare} and $E_{tot}^{F(orH)}$ are the total energies of F (or H)-passivated ABNNR, bare ABNNR and isolated F (or H) atom respectively; x is the number of F (or H) atoms present in the ribbon structures under investigation. The calculated values of E_b for all three considered F (or H)-passivated armchair ribbons, with varying ribbon width, are summarized in Table II and the values in brackets are corresponding to H-passivation. It is to be noted that lower E_b represents higher stability. The perusal of Table II indicates that irrespective of their width $ABNNR_{FB}$ structures are energetically most stable with lowest E_b amongst all considered F-passivated ribbon configurations whereas in case of H-passivation; $ABNNR_{HB}$ are found to be less stable relative to their remaining H-passivated counterparts (i.e., $ABNNR_{HN}$ and $ABNNR_{HBN}$). Though $ABNNR_{HB}$ are also half-metallic³⁷, however, this comparative analysis between F and H-passivated ABNNRs reveals that the possibility of achieving spin polarized transport experimentally is more favorable in edge-fluorinated ABNNRs ($ABNNR_{FB}$) than that of edge-hydrogenated ones ($ABNNR_{HB}$). Thus, being energetically most favorable ribbon structures amongst all presently investigated edge-fluorinated ABNNRs, the results for all $ABNNR_{FB}$ structures are addressed with greater detail (relative to other counterparts) in rest of the text.

3.2 Electronic and transport properties

The calculated electronic band structure and density of states (DOS) along with the Transmission spectrum (TS)^{11,16} for 9- $ABNNR_{FB}$ (as a representative case) are illustrated in figures 2 (a), 2 (b) and 2 (c) respectively. A substantial difference in the form of large splitting of spin states can be

clearly observed in the band structures as well as in DOS profile and TS. The spin-down states are metallic as red bands [figure 2 (a)] are crossing the Fermi level near the zone center and zone boundary whereas owing to the existence of a large band gap of about 4.75 eV spin-up (black) states exhibit insulating behavior. A small peak in transmission coefficient ($TC=3$) corresponding to spin down transmission channels is observed [figure 2 (c)] across the Fermi level which points towards the presence of conducting channels for spin down electrons whereas an energy window of about 4.5 eV corresponding to spin up transmission states (i.e., separation between spin up transmission states across Fermi level) indicates towards the unavailability of conducting paths for spin up electrons. In addition, the absence of mirror symmetry¹⁶ between up and down spin DOS/transmission states [figure 2 (b) and 2 (c)] is correlated with the splitting of spin states as observed in band structure ABNNR_{FB} structures [figure 2 (a)]. Thus, we predict, on the basis of electronic band structure [figure 2 (a)], that the charge transport across the Fermi level through all ABNNR_{FB} structures will be completely dominated by the spin-down electrons as it is evident also from DOS profile and TS [figures 2 (b) and 2 (c)] in terms of – (i) crossing of Fermi level by a peak corresponding to spin-down states and (ii) large separation (> 4 eV) between spin up DOS/ transmission states across Fermi level (i.e. spin up conduction band minima (CBM) and spin up valence band maxima (VBM)). Therefore, it is expected that the current flow through such systems should be entirely spin polarized. Moreover, a half-metal gap (i.e. the gap between top most occupied spin-up band (α' for present case) and Fermi level³⁰) of about 0.21 eV has been witnessed which is high enough for a room temperature device operation as it is sufficiently large than that of the room temperature thermal energy (26 meV) and it is also comparable to the earlier reported values for half-metallic ZBNNRs and GNRs^{30,44}.

Figure 3 (a), 3(b) and 3 (c) respectively display the electronic band structures along with the corresponding DOS and TS for ABNNR_{FBN} configurations. It is obvious from figure 3 (a) that ABNNR_{FBN} are insulating ($E_g > 4.2$ eV) in nature with degenerate electronic bands. The DOS profile also support this insulating behavior in terms of a large separation between the peaks of corresponding spins across Fermi level. The TS, as depicted in figure 3(c), exhibits complete absence of conduction channels around Fermi level as the value of TC is zero across green dotted line and the large separation of transmission states of corresponding spins across Fermi level points towards the existence of a wide band gap in ABNNR_{FBN} structures. The width dependence of band gap for ABNNR_{FBN} structures is illustrated in the inset of figure 3 (a). An oscillating

behavior of band gap with increasing ribbon width is observed for $ABNNR_{FBN}$ structures which is a characteristic signature of $ABNNRs$ ¹⁵. Moreover, the mirror symmetry in the peaks of opposite spin as appearing in the DOS and transmission states [figure 3(b) and 3(c)], is due to preserved spin degeneracy. In contrary, $ABNNR_{FN}$ shows breaking of spin degeneracy as depicted in the corresponding band structure [figure 4(a)] which is further supported by corresponding DOS profile and TS [figure 4(b) and 4(c)]. All $ABNNR_{FN}$ structures, regardless of their width, exhibit a spin dependent wide band gap; an example of 9- $ABNNR_{FN}$ is shown in figure 4 as a representative case.

Now, with this brief discussion on electronic and transport properties, we again come back to half-metallic and energetically most favorable ribbons (i.e. $ABNNR_{FB}$) amongst all presently investigated configurations. In order to understand the origin of half-metallicity in $ABNNR_{FB}$ structures, we analyzed that how the passivation of edge atoms affects the band structure and DOS. The passivation of edge N atoms with F mainly shifts α band away from the Fermi level while change in the position of β band depends also upon passivation of edge-B atoms (figures 2-4). Projected DOS (PDOS) analysis reveals that both of these bands are predominantly composed of $2p$ orbital of unpassivated edge N atoms. Moreover, we have estimated the bare on site Coulombic repulsion^{31,45} as a difference between the first order ionization energy and electron affinity^{31,46} for each element individually. The estimated values are 14.01 eV for F, 8.02 eV for B and 14.79 eV for N. This large difference (≥ 5.99 eV) between N/F and B atoms inhibits the charge transfer through edge-B atoms/B-F bond; therefore, the electrons are localized only in $2p$ orbital of N atoms. This mechanism for origin of half-metallicity is consistent with PDOS analysis and previous reports^{31,47} on $BNNRs$.

3.3 Partial charge analysis (Bloch states analysis)

In order to confirm the localization of charges (which is associated with the origin of presently observed half-metallic nature of $ABNNR_{FB}$) in unpassivated edge-N atoms of $ABNNR_{FB}$, Bloch states have been calculated and the same has been shown in figure 5. The structure of 9- $ABNNR_{FB}$ [figure 1 (a)] consists of 27 B, 27 N and 6 F atoms. A single B (N) atom contributes three (five) valence electrons as its electronic configuration is $2s^22p^1$ ($2s^22p^3$) whereas a single F atom has seven valence electrons - $2s^22p^5$. Thus there are total 258 valence electrons in the system. Moreover, each band is doubly degenerated (considering spin) and hence

there will be a total of 129 valence bands. Therefore, the band index which we used in calculations for VBM is 128 (α band) and 129 (β band) for CBM as indexing starts from zero. For convenience, the spin-down band existing just below (above) α (β) band [figure 2 (a)], is designated as $(\alpha-1)$ [$(\beta+1)$] band. The band index of spin-down $(\alpha-1)$ and $(\beta+1)$ bands are 127 and 130 respectively whereas the band index for spin up α' and β' bands are 126 and 131 respectively. The presented Bloch states calculations are performed for k-points value of (0.0, 0.0, 0.5). In order to keep the size of figures in presentable format, the contour and isosurface of 9-ABNNR_{FB} for α , β , $(\alpha-1)$ and $(\beta+1)$ bands are shown only with one third of the unit cell as depicted in figure 5(a) and 5(b) respectively. For a clear view, the results of β band are also presented with complete unit cell which is used for calculations. It is clear that the Bloch states (red and dark yellow orbitals) corresponding to $(\alpha-1)$ and $(\beta+1)$ bands are completely distinguishable as no mixing of red and yellow orbitals is present in corresponding isosurface [figure 5 (b)]. Similar results are obtained for spin up α' and β' bands of ABNNR_{FB} structures (not shown). These results are also consistent for ABNNR_{FN} and ABNNR_{FBN} (not shown) as none of the bands crosses Fermi level in both of these ribbon configurations. Moreover, the contour and isosurface (for α and β bands particularly) are almost identical (considering charge localization) as both of these bands are correspond to the same spin state (downspin) present across the Fermi level. It can be observed from contour and isosurface plots that the unpaired electrons are mainly localized at the unpassivated edge-N atoms. This charge localization suggests that dangling bond of the edge N-atoms is mainly responsible for observed half-metallic behavior of ABNNR_{FB} structures. In addition, the interchanged colors of Bloch states for α and β bands, at top ribbon edge (as shown by solid black arrows), probably points towards a distinct separation of the corresponding bands (α and β) with Fermi level as it is also similar to the case of interchanged colors of Bloch states (as indicated by dotted black arrows) corresponding to $(\alpha-1)$ and $(\beta+1)$ bands which are well separated with Fermi level [figure 2(a)]. Conversely, colors, at the bottom ribbon edge (as displayed with solid violet arrows), are same for α and β bands which points towards the encroachment of α band (β band) into CB (VB). This suggests that the metallic behavior for spin down states is mainly associated with the localized charge present at unpassivated edge N-atoms due to the unpaired electrons. Moreover, it can be seen that a little charge localization is also appearing around F and near edge N atoms but it has no contribution across the Fermi level as confirmed via PDOS analysis. In addition, the distance between any two adjacent edge N atoms (~ 2.43 Å) is large enough to ensure that no intense edge

reconstruction is taking place (note-occurrence of which could have resulted into two or more dangling bonds per edge-N atom) due to minimum separation between any two adjacent edge N atoms and consequently only one dangling bond is present per edge-N atom. Thus, the present partial charge analysis (Bloch states analysis) suggests that the half-metallic spin polarization in $ABNNR_{FB}$ structures is entirely attributed to the localization of unpaired electrons at unpassivated edge-N atoms.

Further, we calculated electron density for $ABNNR_{FB}$ and $ABNNR_{FN}$ structures. The real space distribution of calculated electron density for $ABNNR_{FB}$ and $ABNNR_{FN}$ structures is depicted in figure 6 and figure S1 (supplementary information) respectively. It has been observed from these figures that for $ABNNR_{FB}$, electron densities corresponding to spin up electrons are almost identical for all N atoms present in the ribbon whereas for spin down electrons the density at unsaturated edge N-atoms is different (as indicated by arrows) than that of all other N atoms present in the same ribbon with almost identical electron densities. This suggests that in case of $ABNNR_{FB}$, spin down electrons present at unsaturated edge N-atoms are responsible for conduction as also confirmed through corresponding band structure, DOS and TS. It is noticeable that in case of $ABNNR_{FN}$, for all atoms present in the ribbon, the electron density is found to be almost identical irrespective of electron spins (figure S1 of supplementary information) which supports to the separation of electronic states across Fermi level as also validated through corresponding band structure, TS and DOS. Present analysis of real space distribution of spin dependent electron densities suggest that the possibility of half-metallic spin polarization in $ABNNR_{FB}$ structures is completely attributed to the localization of unpaired electrons at unsaturated edge-N atoms.

3.4 Magnetic Properties

Since, the stable magnetic state of the material is important from the perspective of spin polarized transport; therefore, we have analyzed the effect of different kinds of edge F-passivation on magnetic properties of ABNNRs. The magnetic properties like magnetic moment for all presently studied ABNNRs have been determined through Mullikan population calculations¹¹ and the calculated magnetic moment M (μ_B) along with the energy difference ΔE (eV) between spin polarized (E_{LSDA}) and spin compensated states (E_{LDA}) for the most stable edge

fluorinated ribbon configuration ($ABNNR_{FB}$) are presented in Table III. A noteworthy net magnetic moment of about $2.03 \mu_B$ is observed for all $ABNNR_{FB}$ structures. In addition, a net magnetic moment of about $2.02 \mu_B$ is also perceived in $ABNNR_{FN}$. On the contrary, any of the $ABNNR_{FBN}$ structures does not exhibit any magnetism. It is worth noticing here that the latter magnetic moment probably have little practical significance as it is observed in $ABNNR_{FN}$ structures which are less stable than that of $ABNNR_{FB}$ structures as confirmed through E_C and E_b analysis. Present non- d orbital type magnetism observed in $ABNNR_{FB}$ structures is accounted due to the magnetic moment of unpaired electrons localized in unpassivated edge-N atoms. This is consistent with giant splitting of spin states [figure 2] and localization of electrons as discussed in Bloch state analysis. It is clear from Table III that the spin polarized state is ~ 0.4 eV ($\Delta E = |E_{LSDA} - E_{LDA}|$) more stable with respect to the spin compensated state (E_{LDA}). This difference is large enough for room temperature device applications and it is also comparable to the values (0.17 eV, 48 meV and 3.5 meV) reported previously^{30,33,35} for ZBNNRs. This significant energy difference offers a strong possibility for presently studied half-metallic $ABNNR_{FB}$ structures to be used as potential candidates for inorganic spintronic device applications. Moreover, the coupling between electrons of inter-edge unpassivated N atoms may be either ferromagnetic or antiferromagnetic, as the observed energies are very close to each other³⁵. Ultimately, we reveal that electronic and magnetic properties of ABNNRs critically depend on the type of edge fluorination, as summarized in Table IV.

4. CONCLUSIONS

Conclusively, the effect of edge fluorination on the electronic and magnetic properties of ABNNRs has been investigated systematically using ab-initio calculations. $ABNNR_{FB}$ are found to be half-metallic and energetically most favorable, with a half-metal gap of 0.21 eV. The spin polarized states are found to be more stable by an energy of ~ 0.4 eV as compared to spin compensated states (E_{LDA}) which projects these half-metallic ribbons as promising building blocks for inorganic spin based electronic (spintronic) devices. Importantly, present stability analysis suggests that the possibility of experimental realization of spin polarized transport is more favorable via edge-fluorination than that of the edge hydrogenation. Moreover, passivation of only edge-B (N) atoms with F atoms i.e. $ABNNR_{FB}$ ($ABNNR_{FN}$) transforms insulating bare ABNNRs into half-metal (wide band gap semiconductor) and gives rise to a substantial magnetic moment of about 2.03 (2.02) μ_B . Conversely, both-edge F-passivation ($ABNNR_{FBN}$) does not

alter electronic or magnetic behavior significantly; therefore, ABNNR_{FBN} structures are insulators with degenerate/symmetric spin states. Owing to the possibility of promising potential of spin polarization, we expect experimental realization of half-metallicity in ABNNRs via edge fluorination.

ACKNOWLEDGMENTS

The authors are thankful to Computational Nanoscience and Technology Laboratory (CNTL), ABV—Indian Institute of Information Technology and Management Gwalior (India) for providing computational facility. One of the authors (HMR) acknowledges the Ministry of Human Resource Development (MHRD), government of India for providing financial support as Teaching Assistantship.

REFERENCES:

- 1 W. Auwärter, H. U. Suter, H. Sachdev and T. Greber, *Chem. Mater.*, 2003, **16**, 343–345.
- 2 D. Pacilé, J. C. Meyer, Ç. Ö. Girit and A. Zettl, *Appl. Phys. Lett.*, 2008, **92**, 133107.
- 3 W.-Q. Han, L. Wu, Y. Zhu, K. Watanabe and T. Taniguchi, *Appl. Phys. Lett.*, 2008, **93**, 223103.
- 4 Y. Lin and J. W. Connell, *Nanoscale*, 2012, **4**, 6908–6939.
- 5 L. H. Li, E. J. G. Santos, T. Xing, E. Cappelluti, R. Roldán, Y. Chen, K. Watanabe and T. Taniguchi, *Nano Lett.*, 2015, **15**, 218–223.
- 6 L. H. Li, J. Cervenka, K. Watanabe, T. Taniguchi and Y. Chen, *ACS Nano*, 2014, **8**, 1457–1462.
- 7 Y. Wang and Y. Ding, *J. Phys. Condens. Matter*, 2014, **26**, 435302.
- 8 Z.-G. Chen, J. Zou, G. Liu, F. Li, Y. Wang, L. Wang, X.-L. Yuan, T. Sekiguchi, H.-M. Cheng and G. Q. Lu, *ACS Nano*, 2008, **2**, 2183–2191.
- 9 L. Li, L. H. Li, Y. Chen, X. J. Dai, P. R. Lamb, B.-M. Cheng, M.-Y. Lin and X. Liu, *Angew. Chem.*, 2013, **125**, 4306–4310.
- 10 M. Y. Han, B. Özyilmaz, Y. Zhang and P. Kim, *Phys. Rev. Lett.*, 2007, **98**, 206805.
- 11 N. K. Jaiswal and P. Srivastava, *IEEE Trans. Nanotechnol.*, 2013, **12**, 685–691.
- 12 N. K. Jaiswal and P. Srivastava, *Solid State Commun.*, 2012, **152**, 1489–1492.
- 13 P. Srivastava, N. K. Jaiswal and G. K. Tripathi, *Solid State Commun.*, 2014, **185**, 41–46.
- 14 P. Srivastava, N. K. Jaiswal and V. Sharma, *Superlattices Microstruct.*, 2014, **73**, 350–358.
- 15 X. Wu, M. Wu and X. C. Zeng, *Front. Phys. China*, 2009, **4**, 367–372.
- 16 H. M. Rai, N. K. Jaiswal, P. Srivastava and R. Kurchania, *J. Comput. Theor. Nanosci.*, 2013, **10**, 368–375.
- 17 Z. Zhang, W. Guo and B. I. Yakobson, *Nanoscale*, 2013, **5**, 6381–6387.
- 18 X. Lin and J. Ni, *Phys. Rev. B*, 2011, **84**, 075461.
- 19 Y. Liu, X. Wu, Y. Zhao, X. C. Zeng and J. Yang, *J. Phys. Chem. C*, 2011, **115**, 9442–9450.
- 20 C. León and A. Latgé, *Phys. Rev. B*, 2013, **88**, 245446.
- 21 X. Li, X. Wu and J. Yang, *J. Am. Chem. Soc.*, 2014, **136**, 5664–5669.
- 22 R. A. de Groot, F. M. Mueller, P. G. van Engen and K. H. J. Buschow, *Phys. Rev. Lett.*, 1983, **50**, 2024–2027.
- 23 V. Alijani, J. Winterlik, G. H. Fecher, S. S. Naghavi and C. Felser, *Phys. Rev. B*, 2011, **83**, 184428.
- 24 K.-I. Kobayashi, T. Kimura, H. Sawada, K. Terakura and Y. Tokura, *Nature*, 1998, **395**, 677–680.

- 25 K.-I. Kobayashi, T. Kimura, Y. Tomioka, H. Sawada, K. Terakura and Y. Tokura, *Phys. Rev. B*, 1999, **59**, 11159–11162.
- 26 I. Galanakis and P. Mavropoulos, *Phys. Rev. B*, 2003, **67**, 104417.
- 27 W.-H. Xie, Y.-Q. Xu, B.-G. Liu and D. G. Pettifor, *Phys. Rev. Lett.*, 2003, **91**, 037204.
- 28 B.-G. Liu, in *Half-metallic Alloys*, eds. I. Galanakis and P. H. Dederichs, Springer Berlin Heidelberg, 2005, vol. 676, pp. 267–291.
- 29 M. Jourdan, J. Minár, J. Braun, A. Kronenberg, S. Chadov, B. Balke, A. Gloskovskii, M. Kolbe, H. J. Elmers, G. Schönhense, H. Ebert, C. Felser and M. Kläui, *Nat. Commun.*, 2014, **5**.
- 30 F. Zheng, G. Zhou, Z. Liu, J. Wu, W. Duan, B.-L. Gu and S. B. Zhang, *Phys. Rev. B*, 2008, **78**, 205415.
- 31 Y. Wang, Y. Ding and J. Ni, *Phys. Rev. B*, 2010, **81**, 193407.
- 32 V. Barone and J. E. Peralta, *Nano Lett.*, 2008, **8**, 2210–2214.
- 33 W. Chen, Y. Li, G. Yu, C.-Z. Li, S. B. Zhang, Z. Zhou and Z. Chen, *J. Am. Chem. Soc.*, 2010, **132**, 1699–1705.
- 34 L. Lai and J. Lu, *Nanoscale*, 2011, **3**, 2583–2588.
- 35 D. K. Samarakoon and X.-Q. Wang, *Appl. Phys. Lett.*, 2012, **100**, 103107.
- 36 Z. M. Liu, Y. Zhu and Z. Q. Yang, *J. Chem. Phys.*, 2011, **134**, 074708.
- 37 H. M. Rai, S. K. Saxena, V. Mishra, R. Late, R. Kumar, P. R. Sagdeo, N. K. Jaiswal and P. Srivastava, *Solid State Commun.*, 2015, **212**, 19–24.
- 38 Y. Ding, Y. Wang and J. Ni, *Appl. Phys. Lett.*, 2009, **94**, 233107.
- 39 M. Chattopadhyaya, M. M. Alam, S. Sen and S. Chakrabarti, *Phys. Rev. Lett.*, 2012, **109**, 257204.
- 40 M. Brandbyge, J.-L. Mozos, P. Ordejón, J. Taylor and K. Stokbro, *Phys. Rev. B*, 2002, **65**, 165401.
- 41 J. P. Perdew and A. Zunger, *Phys. Rev. B*, 1981, **23**, 5048–5079.
- 42 J. Zhao, A. Buldum, J. Han and J. P. Lu, *Nanotechnology*, 2002, **13**, 195.
- 43 N. K. Jaiswal, G. Kovačević and B. Pivac, *Appl. Surf. Sci.*, 2015, **357**, Part A, 55–59.
- 44 Y.-W. Son, M. L. Cohen and S. G. Louie, *Nature*, 2006, **444**, 347–349.
- 45 S. Dutta, A. K. Manna and S. K. Pati, *Phys. Rev. Lett.*, 2009, **102**, 096601.
- 46 The data of ionization energy and electron affinity is adopted from http://chemed.chem.purdue.edu/genchem/topicreview/bp/ch7/ie_ea.html.
- 47 F. Zheng, K. Sasaki, R. Saito, W. Duan and B.-L. Gu, *J. Phys. Soc. Jpn.*, 2009, **78**, 074713.

Tables:

Table 1. Calculated cohesive energies (eV) as a function of ribbon width for all considered edge fluorinated ABNNR structures.

Ribbon width N_a	E_c (eV)		
	ABNNR _{FB}	ABNNR _{FBN}	ABNNR _{FN}
6	-9.08	-8.54	-8.56
7	-9.22	-8.73	-8.77
8	-9.33	-8.87	-8.93
9	-9.41	-9.00	-9.06
10	-9.49	-9.10	-9.16

Table 2. Calculated binding energy (eV) per F (or H)-atom as a function of ribbon width for all considered F and H-passivated ABNNR structures; the values in brackets are corresponding to H-passivation.

Ribbon width N_a	E_B (eV)		
	$ABNNR_{FB(HB)}$	$ABNNR_{FBN(HBN)}$	$ABNNR_{FN(HN)}$
6	-6.406 (-3.489)	-5.588 (-5.184)	-2.792 (-4.178)
7	-6.424 (-3.493)	-5.594 (-5.188)	-2.804 (-4.189)
8	-6.416 (-3.486)	-5.591 (-5.186)	-2.797 (-4.184)
9	-6.418 (-3.482)	-5.592 (-5.187)	-2.800 (-4.186)
10	-6.417 (-3.482)	-5.592 (-5.187)	-2.799 (-4.185)

Table 3. Calculated magnetic moment and energy difference ($\Delta E = |E_{LSDA} - E_{LDA}|$) between spin polarized and spin un-polarized states for most stable $ABNNR_{FB}$ structures with varying ribbon width.

	$N_a=6$	$N_a=7$	$N_a=8$	$N_a=9$	$N_a=10$
M (μ_B)	2.03	2.04	2.03	2.03	2.03
ΔE (eV)	0.41	0.38	0.40	0.42	0.41

Table 4. The overall magnetic and electronic behavior for all considered edge fluorinated ABNNRs ($N_a=6$ to 10).

Ribbon Configuration	Avg. M (μ_B)	Electronic state	Band gap (eV)	Magnetic behavior
$ABNNR_{FB}$	2.03	Half-metal (0.21 eV)	0	Magnetic
$ABNNR_{FBN}$	0	Insulator	4.26 to 4.38	Non- magnetic
$ABNNR_{FN}$	2.02	Wide band gap Semiconductor	3.16 to 3.34	Magnetic

Figures:-

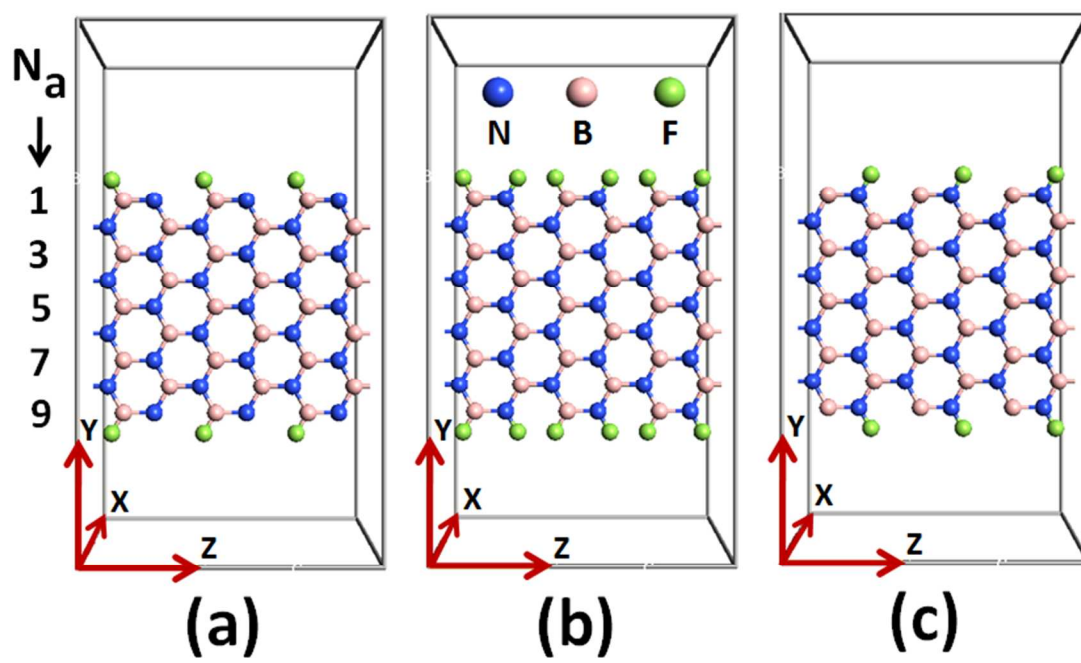
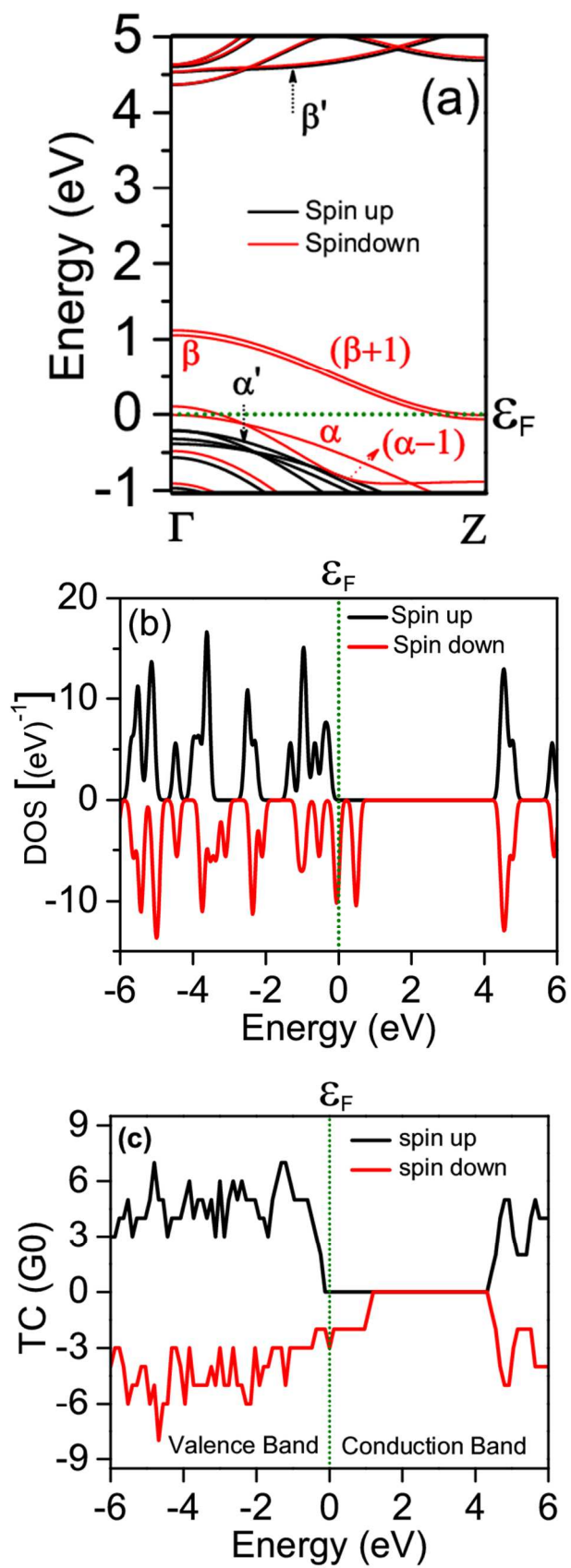
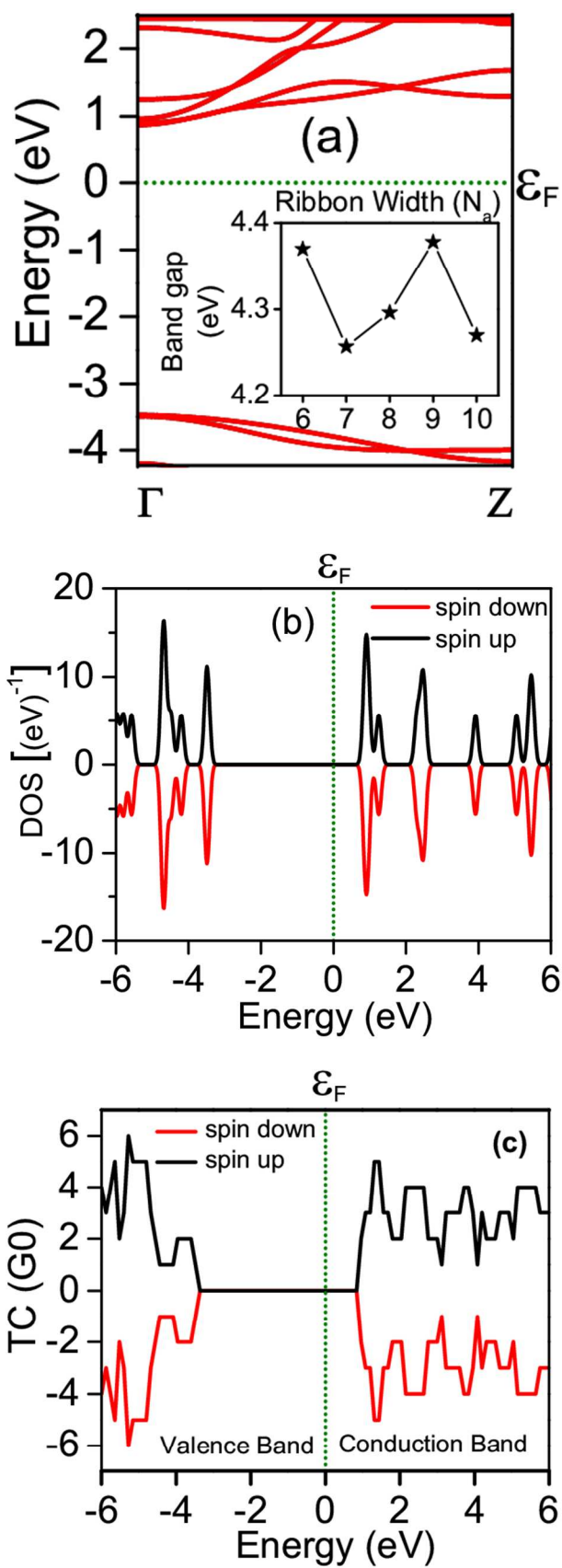
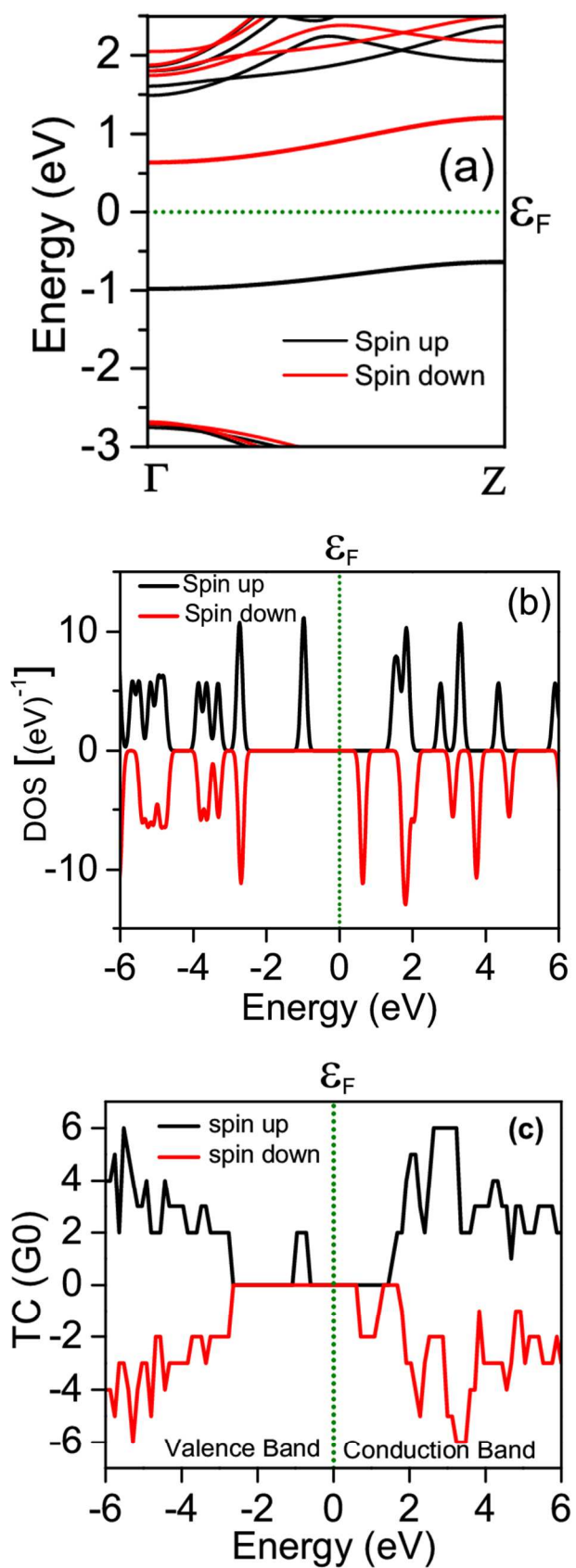


Figure 1

**Figure 2**

**Figure 3**

**Figure 4**

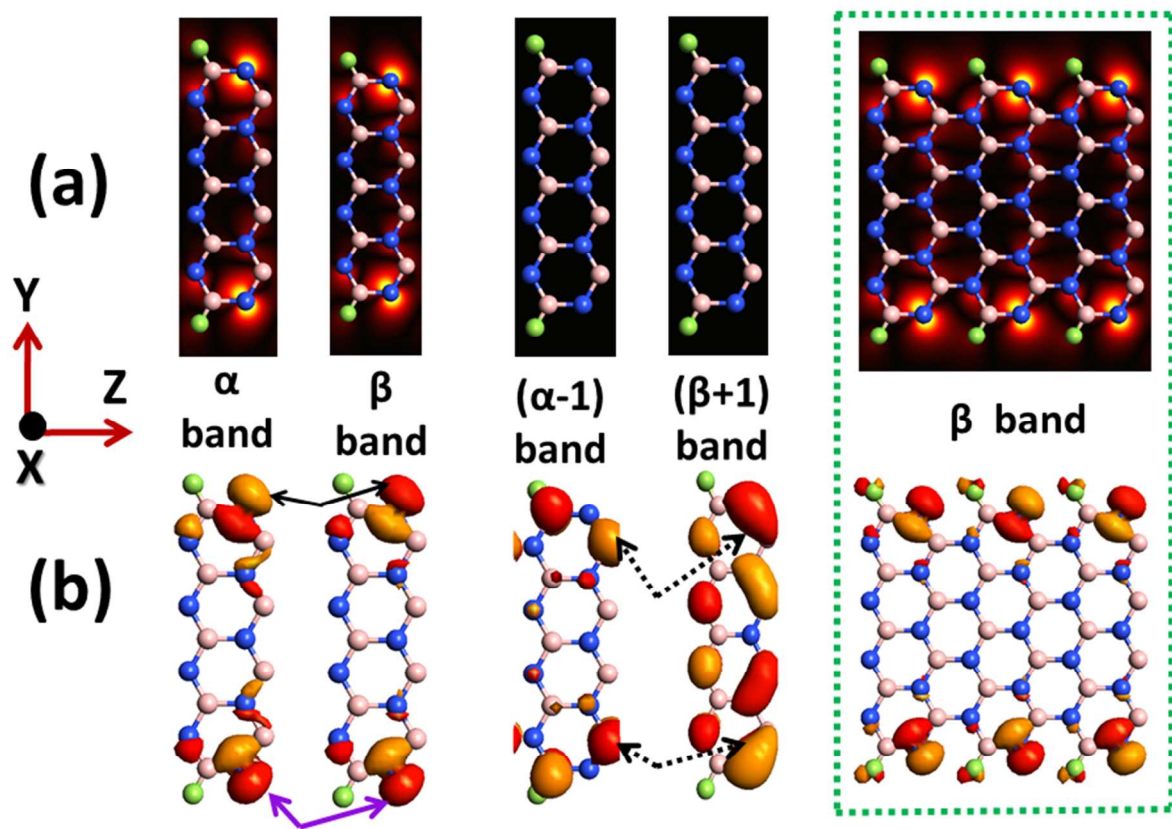


Figure 5

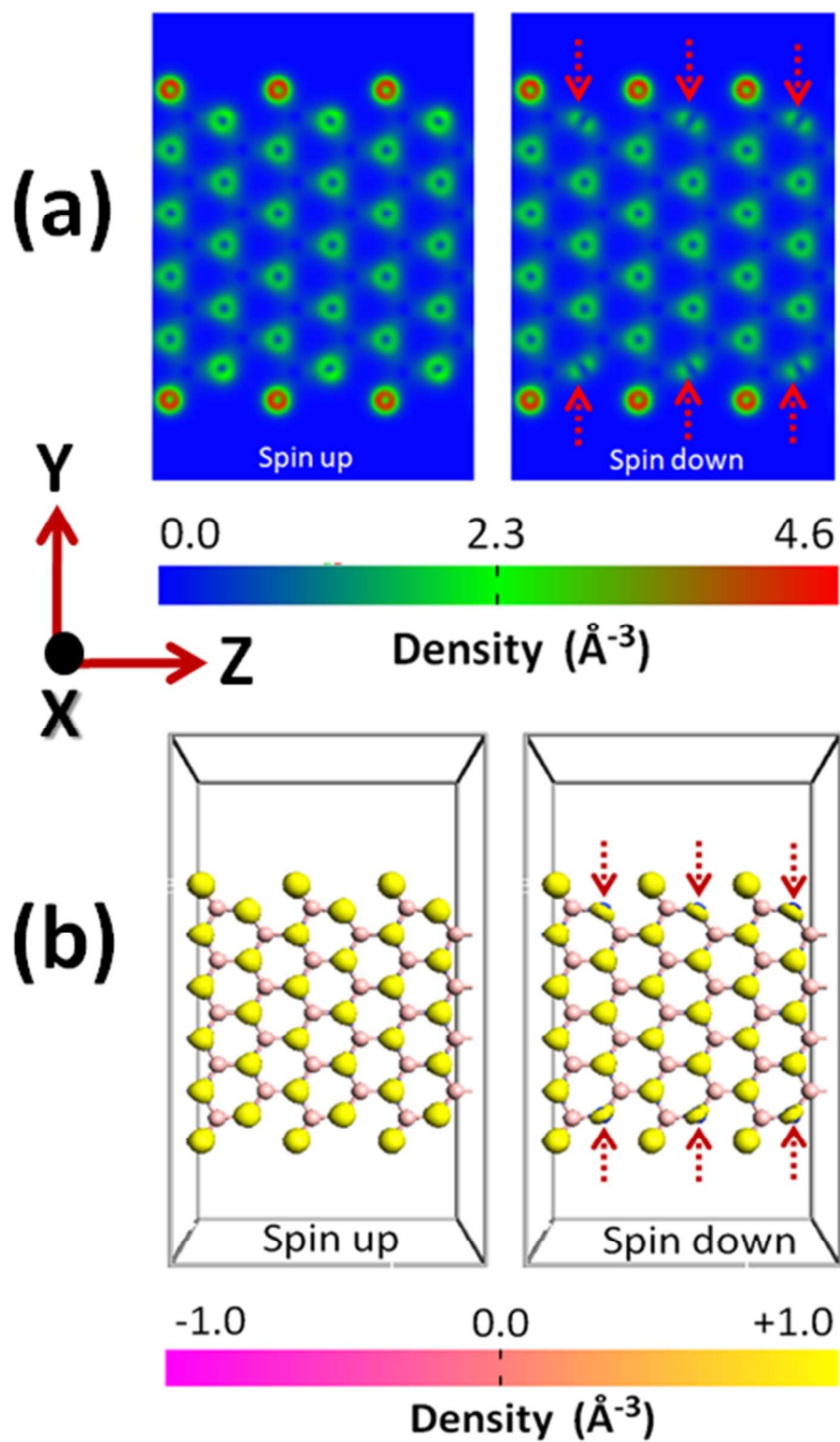


Figure 6

Figure Captions:

FIG. 1 (Color online). Convention of ribbon width and the supercell units ($N_a=9$ as a representative) for (a) ABNNR_{FB}, (b) ABNNR_{FBN} and (c) ABNNR_{FN}. The ABNNRs are modeled with periodic boundary conditions along z - axis whereas x and y directions are confined.

FIG. 2 (Color online). Half-metallic behavior of 9-ABNNR_{FB}; calculated (a) electronic band structure and (b) density of states (DOS) and (c) transmission spectrum (TS) for 9-ABNNR_{FB}. In (a), spin down (spin-up) states nearest to the Fermi level in valence band and conduction band are indexed with α (α') and β (β') respectively. The Fermi level is indicated by green dotted line whereas spin down (spin-up) states are shown with red (black) color.

FIG. 3 (Color online). Spin degeneracy and insulating nature of 9-ABNNR_{FBN}; Calculated (a) electronic band structure and (b) density of states (DOS) and (c) transmission spectrum (TS) for 9-ABNNR_{FBN}. The Fermi level is indicated by green dotted line whereas spin down (spin-up) states are shown with red (black) color.

FIG. 4 (Color online). Calculated (a) electronic band structure and (b) density of states (DOS) and (c) transmission spectrum (TS) for 9-ABNNR_{FN}. The Fermi level is indicated by green dotted line whereas spin down (spin-up) states are shown with red (black) color.

FIG. 5 (Color online). Calculated Bloch states for spin down α , β , ($\alpha-1$), ($\beta+1$) bands and spin up α' and β' bands of 9-ABNNR_{FB} are presented in the form of (a) Contour and (b) Isosurface. The isovalue is 0.09 (au). To keep the size of figure in a presentable format only one third (along z - axis) of actual unit cell is shown and for a clear view, the results corresponding to β band are presented also with actual ribbon geometry (enclosed in a dotted rectangle) which is used for calculations. The ABNNRs are modeled with periodic boundary conditions along z - axis whereas x and y directions are confined.

FIG. 6 (Color online). The real space distribution of calculated electron densities corresponding to spin up and spin down electrons for 9-ABNNR_{FB} is presented in the form of (a) Contour and (b) Isosurface. The corresponding density scale is shown by a tricolored rectangular horizontal strip situated at the bottom. In figure (b), the electron density is plotted corresponding to isovalue 1 (au). In order to display the distinct change between spin up and spin down electron densities at ribbon edges, ribbon configurations are not shown in figure (a). B and N atoms are same in shape, size and color as that of represented in figure 1. The ABNNRs are modeled with periodic boundary conditions along z - axis whereas x and y directions are confined.